J. Plasma Physics (1999), *vol.* 62, *part* 4, *pp.* 367–388. Printed in the United Kingdom

Two-dimensional semi-Lagrangian Vlasov simulations of laser–plasma interaction in the relativistic regime

M. L. BÉGUÉ,[1] A. GHIZZO,[1] P. BERTRAND,[1]
E. SONNENDRÜCKER[2] and O. COULAUD[2]

[1] Laboratoire de Physique des Milieus Ionisés, UPRES A 7040, and
[2] Institut Elie Cartan de Nancy, Université Henri Poincaré Nancy I, BP 239,
54 506 Vandoeuvre les Nancy, Cedex, France

(Received 8 June 1998 and in revised form 26 April 1999)

Abstract. A semi-Lagrangian two-dimensional fully relativistic Vlasov code for multicomputer environments is developed to study trapped-particle dynamics in phase space induced by relativistic modulational and Raman instabilities. Attention is focused on the efficiency properties of the numerical scheme, which allows a very fine description of particle dynamics in phase space. Vlasov simulations show the appearance of coherent vortex structures as a result of the nonlinear saturation mechanism of the relativistic modulational instability. Growth rates are computed and found to be in good agreement with theoretical values obtained from the dispersion relation by Quesnel et al, [*Phys. Plasmas* **4**, 3358–3368 (1997)] and Guérin et al. [*Phys. Plasmas* **2**, 2807–2814 (1995)]. In the case of coupling between the relativistic modulational instability and two-plasmon decay, stochastic behaviour can be observed due to the competition between different plasmas waves.

1. Introduction

As a result of recent progress in optical processing, lasers reaching petawatt power are becoming available, yielding intensities ranging from 10^{17} to 10^{20} W cm^{-2} for which relativistic effects become significant for electron. The interaction of such laser beams with moderately underdense to slightly overdense plasmas is of particular interest in the 'fast ignitor' context and advanced accelerators. As these high-intensity lasers have very short pulses (< 1 ps), ion motion can be neglected, so that we only need to consider electron parametric instabilities. At moderate intensities, these instabilities are clearly identified as stimulated Raman scattering (SRS), relativistic modulational instability (RMI), relativistic filamentation instability (RFI) and two-plasmon decay (TPD). SRS is a resonant three-wave coupling process where an electromagnetic pump wave (EMW) decays into an electron plasma wave (EPW) and a scattered light wave. SRS occurs for $n \leqslant \frac{1}{4}n_c$, where n is the electron plasma density and $n_c = m_e\varepsilon_0\omega_0^2/e^2$ is the critical density associated with the laser pump frequency ω_0. On the other hand, TPD (also called $2\omega_p$) is a three-wave interaction process where the transversely polarized electromagnetic pump wave decays into two EPW, which are longitudinally polarized. In order to have frequency matching between the pump and both EPW daughter waves, we

must have $\omega_0 = \omega_1 + \omega_2 \approx 2\omega_p$ i.e. $\omega_{EPW} \approx \frac{1}{2}\omega_0$, which means that TPD can only occur near the quarter-critical density layer, where the density is $\frac{1}{4}n_c$.

In fact, SRS and TPD are both high-frequency three-wave parametric instabilities. In both cases, the pump wave is transversely polarized. That is, the pump wave's electric field is strictly perpendicular to its propagation or **k** vector. For both SRS and TPD, one of the two daughter waves is longitudinally polarized (no vector potential can be associated with this wave). For SRS, the second daughter wave is assumed to be transversely polarized, while for TPD, the second daughter wave is assumed to be longitudinally polarized. The mixed polarization instability has recently been studied by Afeyan and Williams (1997a,b) and is a generalization that has SRS and TPD as special cases (the authors examine circumstances where the polarization of the second daughter wave is not restricted to be either longitudinal or transverse, but is taken to be an arbitrary admixture of the two).

In the fully relativistic regime, the one-dimensional (1D) dispersion relation has been established recently by Guérin et al. (1995) for a plasma of any density, including the so-called induced transparency regime $n_c \leqslant n \leqslant \gamma_0 n_c$, where γ_0 is the relativistic factor of the electron oscillating in the electric field of the laser wave. Its analytical and numerical solution shows a wide variety of regimes, depending on the parameter $p_{\rm osc}$ (quiver momentum) and n/n_c. The two-dimensional (2D) fully relativistic case has been studied by Quesnel et al. (1997a,b) by solving the dispersion relation of the electron parametric instability of a circularly polarized wave in a cold plasma at any laser intensity and plasma density. The authors have identified different regimes, and in particular the existence of unstable modes at high values of $k_\perp$ (the wave vector component perpendicular to the incident pump wave vector $\mathbf{k}_0$). In the relativistic regime, the unstable wavenumber area may extend to high values of $k_\perp$ with high growth rates. At ultrahigh $k_\perp$, TPD and RMI tend to merge. In the fully relativistic regime (corresponding to RMI), generally obtained with a large-amplitude electromagnetic wave with an irradiance of a few $10^{18}\,\mathrm{W\,cm^{-2}}$, the Lorenz force is no longer negligible, and the EPW can reach the wavebreaking limit.

An obvious way to improve the understanding of relativistic particle trapping, plasma wavebreaking and/or particle acceleration is to use semi-Lagrangian codes (Ghizzo et al. 1995; see also Bertrand et al. 1990), where (unlike 'particles-in-cell', PIC, codes) the phase-space resolution is guaranteed, regardless of phase-space particle density. Such Vlasov codes render possible a detailed examination of the low-density regions of phase space, especially the description of the tail phenomena where only a small number of electrons are involved. In this type of problems, PIC codes suffer from poor statistics. This because they lack a sufficient number of simulation particles to display the detailed phase-space structure of the distribution function, which is often obtained in those regions of phase space where particle and phase velocities are comparable and where trapping or wavebreaking occurs.

In the present paper, examples of TPD and RMI simulations are given using semi-Lagrangian 1D and 2D Vlasov codes. Details of the semi-Lagrangian method are given in Begué et al. (1998) and Coulaud et al. (1999), where we discuss the parallelization of the 2D electrostatic Vlasov code on a distributed memory architecture. The paper is organized as follows. Section 2 describes an example of a 1D Vlasov simulation at high laser intensity corresponding to $p_{\rm osc}/mc = \sqrt{3}$ and $n/n_c\gamma_0 = 0.25$ related to RMI. Then we present our 2D Vlasov model in Sec. 3.

https://doi.org/10.1017/S0022377899008065 Published online by Cambridge University Press

Section 4 emphasizes the results of Vlasov simulation concerning the RMI process in two dimensions without TPD coupling, which is treated in Sec. 5. Finally, our conclusions are given in Sec. 6.

2. 1D Vlasov simulations of RMI

2.1. Basic equations

We limit our discussion here to a 1D model, which precludes the TPD and Raman side-scattering instability but retains SRS and longitudinal RMI when a large-amplitude electromagnetic pump wave is considered. We choose here a couple of parameters close to $n/n_c = 0.5$ and $p_{\text{osc}}/mc = \sqrt{3}$ (i.e. $n/\gamma_0 n_c = 0.25$, with a Lorentz factor of $\gamma_0 = \sqrt{1 + p_{\text{osc}}^2/m^2c^2} = 2$). Although the parameters are chosen in the region of the TPD process, the relativistic regime leads to the growth of RMI located around $k_\perp c/\omega_p \approx 0$. In the fully relativistic regime, perturbation theory cannot be used to take account of nonlinearities of the primary wave (thus the case of an electromagnetic wave with linear polarization is more complicated to handle). In order to overcome this difficulty, the nonlinear electromagnetic wave is assumed to be circularly polarized. It is then well known that for such a polarization the amplitude of the electric field and of the electron quiver velocity remain constant.

We start from the 1D2/2 relativistic Vlasov model:

$$\frac{\partial F}{\partial t} + \frac{p_x}{m\gamma_3}\frac{\partial F}{\partial x} + e\left(\mathbf{E} + \frac{\mathbf{p}}{m\gamma_3} \times \mathbf{B}\right)\frac{\partial F}{\partial \mathbf{p}} = 0, \tag{1}$$

with the relativistic factor given by

$$\gamma_3^2 = 1 + \frac{p_x^2 + p_y^2 + p_z^2}{m^2c^2} \tag{2}$$

By considering a class of exact solution of (1) in the form

$$F(x, \mathbf{p}, t) = f(x, p_x, t)\,\delta\left(p_y - P_y(x,t)\right)\delta\left(p_z - P_z(x,t)\right), \tag{3}$$

(1) can be written as

$$\frac{\partial f}{\partial t} + \frac{p_x}{m\gamma_1}\frac{\partial f}{\partial x} + \left(eE_x - \frac{mc^2}{2\gamma_1}\frac{\partial\left(a^2\right)}{\partial x}\right)\frac{\partial f}{\partial p_x} = 0, \tag{4}$$

with the Lorentz factor now given by:

$$\gamma_1^2 = 1 + \frac{p_x^2}{m^2c^2} + a^2(x,t) \tag{5}$$

and where $a(x,t) = eA/mc$ is the normalized amplitude of the vector potential $\mathbf{A} = (0, A_y, A_z)$. Note that the generalized canonical momentum is then given by $\mathbf{P}_\perp + e\mathbf{A}_\perp = 0$. The Vlasov equation is then coupled with the Maxwell equations:

$$\frac{\partial E_y}{\partial t} = -c^2\frac{\partial B_z}{\partial x} + \omega_p^2 A_y \rho, \tag{6}$$

$$\frac{\partial E_z}{\partial t} = c^2\frac{\partial B_y}{\partial x} + \omega_p^2 A_z \rho, \tag{7}$$

$$\frac{\partial B_y}{\partial t} = \frac{\partial E_z}{\partial x}, \tag{8}$$

$$\frac{\partial B_z}{\partial t} = -\frac{\partial E_y}{\partial x}, \tag{9}$$

https://doi.org/10.1017/S0022377899008065 Published online by Cambridge University Press

where

$$\rho(x,t) = \int \frac{f\, dp_x}{m\gamma_1}.$$

The vector potential components are then computed using $\partial \mathbf{A}_\perp / \partial t = -\mathbf{E}_\perp$, and the longitudinal component of the field is obtained by solving the Poisson equation:

$$\frac{\partial E_x}{\partial x} = \frac{e}{\varepsilon_0}\left[n_e(x,t) - n_i\right]. \tag{10}$$

The well-known fractional step or 'splitting scheme' is then used to integrate the distribution function (see Coulaud et al. 1999): we shift the distribution function along the x direction, leading to

$$f^*(x,p_x) = f(x-\alpha, p_x, t_n), \tag{11a}$$

with

$$\alpha = \Delta t\, v\left(x - \frac{\alpha}{2}, p_x, t_{n+1/2}\right), \tag{11b}$$

where v is the function $p_x/m\gamma_1$. Then, in the momentum (p_x) space with the corresponding expression

$$f(x,p_x,t_{n+1}) = f^*(x, p_x - \beta) \tag{12a}$$

with

$$\beta = \Delta t\, w\left(x, p_x - \frac{\beta}{2}, t_{n+1/2}\right) \tag{12b}$$

and

$$w(x,p_x,t) = eE_x - \frac{mc^2}{2\gamma_1}\frac{\partial\left(a^2\right)}{\partial x}. \tag{13}$$

The Maxwell equations are integrated by using the usual leapfrog scheme with time subcycling.

2.2. Numerical results

We consider here a circularly polarized electromagnetic pump wave of frequency $\omega_0 = \sqrt{2}\omega_p$ and wavenumber $k_0 c/\omega_p \approx 1.225$. The ratio of the electron density to the critical density is then $n/n_c = 0.50$, i.e. $n/\gamma_0 n_c = 0.25$. Since in the 1D model the TPD is precluded, RMI starts up in the relativistic regime. Figure 1 shows the growth rate γ/ω_p as a function of the wavenumber kc/ω_p directly obtained by an 1D analysis of the dispersion relation (see e.g. Guérin et al. 1995). RMI reaches a maximum growth rate $\gamma_{\max}/\omega_p \approx 0.562$ at $kc/\omega_p \approx 2.353$, and the corresponding real frequency is close to $\omega/\omega_p \approx 0.47$. To make a comparison with theoretical results, a numerical simulation has been performed with a plasma length box of $L_x = 2\pi/k_0 \approx 5.130\ c/\omega_p$ (the fundamental wavenumber being $\Delta k = k_0$), leading to the appearance of a plasma wave of wavenumber $k_e c/\omega_p \approx 2\Delta k c/\omega_p \approx 2.449$ chosen in the region of maximum RMI growth rate. The phase-space sampling is taken as $N_x = 512$ and $N_{p_x} = 256$. In order to start the instability from the round-off errors of the Vlasov code (the Vlasov code being noiseless), we choose as initial condition

https://doi.org/10.1017/S0022377899008065 Published online by Cambridge University Press

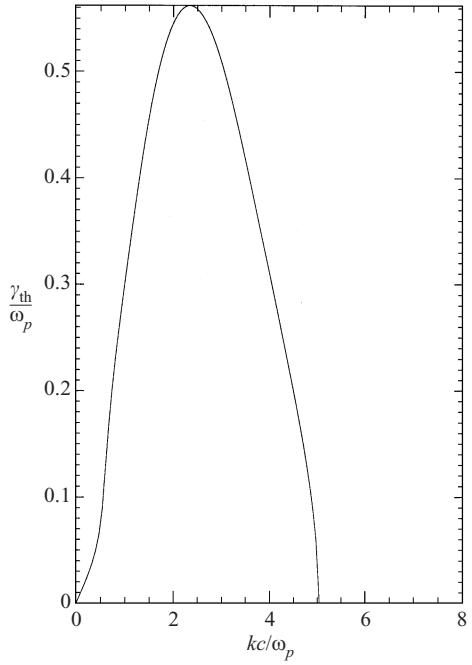

Figure 1. The growth rate γ/ω_p has been plotted as a function of the wavenumber kc/ω_p in the case of RMI by solving the 1D dispersion relation. The parameters are $\omega_0/\omega_p = \sqrt{2}$ (i.e. $n/\gamma_0 n_c = 0.25$) and $p_{\rm osc}/mc = \sqrt{3}$.

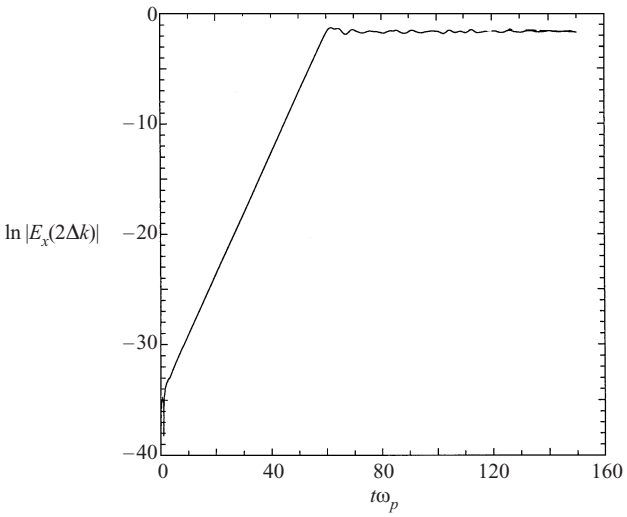

Figure 2. Time evolution of the plasma mode in the Vlasov simulation corresponding to the most unstable modes. The numerical growth rate is found to be $\gamma_{\rm num}/\omega_p \approx 0.550$, which is close to the theoretical value of $\gamma_{RMI}/\omega_p \approx 0.558$.

a Maxwellian distribution function without perturbation and take the following initial conditions to describe the circularly polarized electromagnetic field:

$$\mathbf{E} = (0,\ E_0 \cos k_0 x,\ E_0 \sin k_0 x)\,, \tag{14}$$

https://doi.org/10.1017/S0022377899008065 Published online by Cambridge University Press

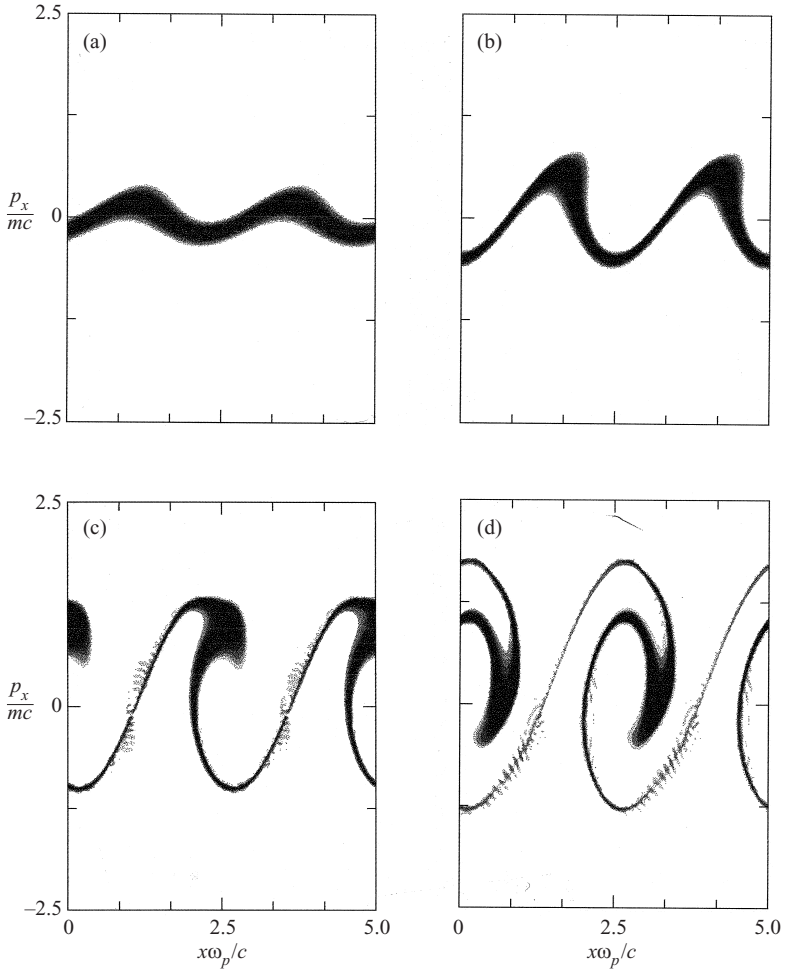

Figure 3 (a–d). For caption see facing page.

$$\mathbf{B} = \left(0,\ -\frac{k_0^* E_0}{\omega_0^*}\sin k_0 x,\ \frac{k_0^* E_0}{\omega_0^*}\cos k_0 x\right), \tag{15}$$

$$\mathbf{P} = \left(0,\ -\frac{eE_0}{\omega_0^*}\sin k_0 x,\ \frac{eE_0}{\omega_0^*}\cos k_0 x\right), \tag{16}$$

where

$$\omega_0^* = \omega_0 \operatorname{sinc}\frac{\omega_0 \Delta t}{2}, \qquad k_0^* = k_0 \operatorname{sinc}\frac{k_0 \Delta x}{2},$$

with

$$\operatorname{sinc} x = \frac{\sin x}{x}.$$

Using the well-known leapfrog scheme to integrate the Maxwell equations (6)–(9), a little algebra leads to a numerical expression for the dispersion relation for circularly polarized electromagnetic waves, $\omega_0^{*2} = \omega_p^2/\gamma_0 + k_0^{*2}c^2$. Figure 2 shows the

https://doi.org/10.1017/S0022377899008065 Published online by Cambridge University Press

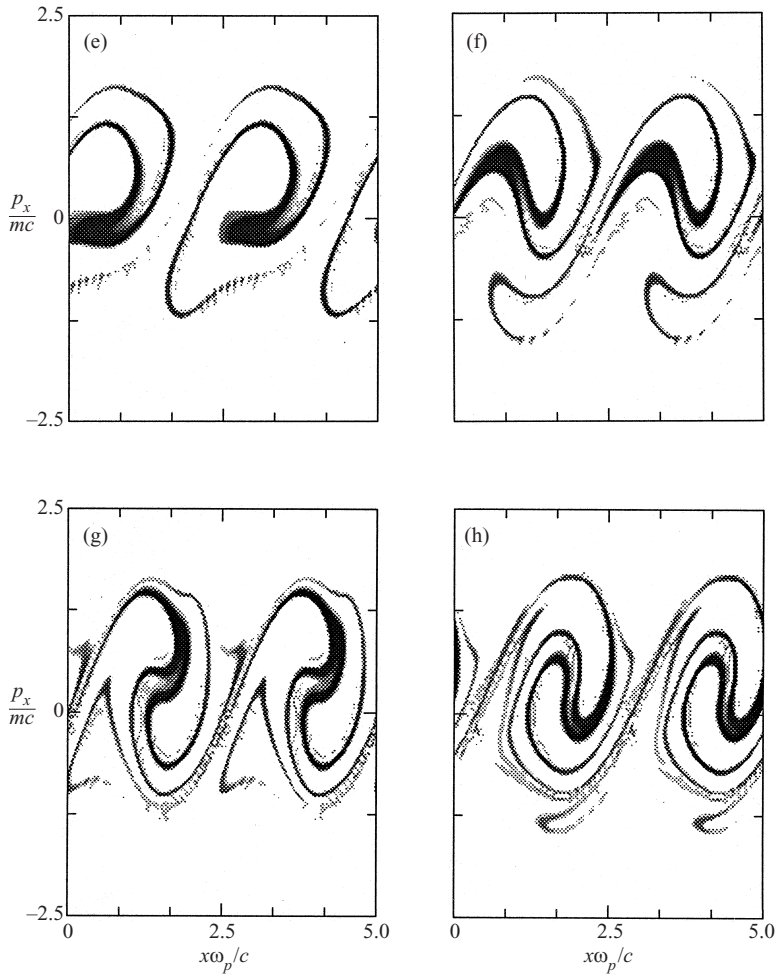

Figure 3. Phase-space representation of the distribution function of RMI using 1D semi-Lagrangian Vlasov simulation. The curves are shown from times $t\omega_p = 58$ (a) until 72 (h) (every $2\omega_p^{-1}$). They clearly show a strong modulation followed by particle trapping in phase space.

time evolution of the plasma-wave mode on a logarithmic scale. The numerical growth rate of this mode is determined by the slope of the curve of Fig. 2, and can be compared with the theoretical predictions given in Fig. 1. The agreement is particularly good: the growth rate value obtained by the 1D Vlasov simulation is $\gamma_{\rm num}/\omega_p \approx 0.550$, which is close to the theoretical value of $\gamma_{RMI}/\omega_p \approx 0.558$. Because of its very fine resolution in phase-space, the Vlasov code is capable of resolving the finest details of particle trapping. As an example, Fig. 3 shows the phase-space representation of the whole distribution function from time $t\omega_p = 58$ until 72 (every $2\omega_p^{-1}$). Figure 3 show clearly the strong modulation of the distribution function followed by particle trapping in the longitudinal field and then the formation of coherent phase-space structures in (x, p_x) phase space as a result of the RMI saturation mechanism.

https://doi.org/10.1017/S0022377899008065 Published online by Cambridge University Press

3. The 2D relativistic Vlasov model

We use 2D semi-Lagrangian electromagnetic Vlasov simulations with circular polarization. In most cases, for simplicity, we again restrict the discussion to the case of fixed ions. Electron parametric instabilities in the relativistic regime have been extensively studied in 1D and extended to 2D problems (see e.g. Quesnel et al. 1997a,b; Adam et al. 1997). The 2D instability involves the coupling of harmonics (see Sakharov et al. 1995), TPD, side-scattering and RFI. In this paper, we limit our study to the RMI–TPD coupling. To model this, we consider an infinite homogeneous plasma in the x and y directions with a pump wavevector in the x direction, all field quantities being functions of the space variables x and y. Choosing the Coulomb gauge $\boldsymbol{\nabla}\cdot\mathbf{A}=0$, the vector potential $\mathbf{A}$ has three components A_x, A_y and A_z. Recalling that $\mathbf{E}=-\boldsymbol{\nabla}\phi-\partial\mathbf{A}/\partial t$, the 2D1/2 electron distribution function $F(x,y,\mathbf{p},t)$ obeys the relativistic Vlasov equation:

$$\frac{\partial F}{\partial t}+\frac{\mathbf{p}}{m\gamma_3}\cdot\frac{\partial F}{\partial \mathbf{r}}+e\left(\mathbf{E}+\frac{\mathbf{p}}{m\gamma_3}\times\mathbf{B}\right)\cdot\frac{\partial F}{\partial \mathbf{p}}=0, \tag{17}$$

where $\mathbf{r}=(x,y,0)$ and $\mathbf{p}=\left(p_x,p_y,p_z\right)$. But huge memory requirements are necessary to handle a full 2D1/2 kinetic model, i.e. five phase-space variables. It is then possible to reduce the number of variables by using the fact that $E_z=-\partial A_z/\partial t$, which is equivalent to taking a class of exact solutions of (17) in the form

$$F\left(x,y,p_x,p_y,p_z,t\right)=f\left(x,y,p_x,p_y,t\right)\delta\left(p_z-P_z\left(x,y,t\right)\right) \tag{18}$$

The reduced 2D distribution function f describing particle motion in the plane now satisfies the 2D reduced Vlasov equation, used in our model:

$$\frac{\partial f}{\partial t}+\frac{p_x}{m\gamma_2}\frac{\partial f}{\partial x}+\frac{p_y}{m\gamma_2}\frac{\partial f}{\partial y}+e\left(E_x+\frac{p_yB_z-P_zB_y}{m\gamma_2}\right)\frac{\partial f}{\partial p_x}$$
$$+e\left(E_y+\frac{P_zB_x-p_xB_z}{m\gamma_2}\right)\frac{\partial f}{\partial p_y}=0, \tag{19}$$

with a new expression for the relativistic factor γ_2 given by

$$\gamma_2^2=1+\frac{p_x^2+p_y^2+P_z^2\left(x,y,t\right)}{m^2c^2}. \tag{20}$$

The transverse momentum P_z is obtained through conservation of the generalized canonical momentum $P_z+eA_z=0$, giving rise to

$$\frac{\partial P_z}{\partial t}=eE_z. \tag{21}$$

Both TE (transverse electric field: E_z,B_x,B_y) and TM (transverse magnetic field: E_x,E_y,B_z) components were taken into account in our model. For TM modes, the Maxwell equations are then given in the well-known form

$$\frac{\partial E_x}{\partial t}=c^2\frac{\partial B_z}{\partial y}-\frac{J_x}{\varepsilon_0}, \tag{22}$$

$$\frac{\partial E_y}{\partial t}=-c^2\frac{\partial B_z}{\partial x}-\frac{J_y}{\varepsilon_0}, \tag{23}$$

$$\frac{\partial B_z}{\partial t}=-\left(\frac{\partial E_y}{\partial x}-\frac{\partial E_x}{\partial y}\right), \tag{24}$$

https://doi.org/10.1017/S0022377899008065 Published online by Cambridge University Press

while, for TE modes,

$$\frac{\partial B_x}{\partial t} = -\frac{\partial E_z}{\partial y} \tag{25}$$

$$\frac{\partial B_y}{\partial t} = \frac{\partial E_z}{\partial x} \tag{26}$$

$$\frac{\partial E_z}{\partial t} = c^2 \left(\frac{\partial B_y}{\partial x} - \frac{\partial B_x}{\partial y} \right) - \frac{J_z}{\varepsilon_0} \tag{27}$$

where the plasma current density is given by

$$\mathbf{J} = \frac{e}{m} \int \int \frac{dp_x \, dp_y \, \mathbf{p} f}{\gamma_2}, \tag{28a}$$

with

$$\mathbf{p} = \left(p_x, p_y, P_z \left(x, y, t \right) \right) \tag{28b}$$

Again the usual leapfrog scheme is used to compute the electromagnetic field at each time step (see Birdsall and Langdon 1995).

4. Results of 2D Vlasov–Maxwell simulations

4.1. Mode analysis

The results presented here were processed on the Cray T3E computing system. A phase-space grid $N_x N_y N_{p_x} N_{p_y}$ of 256×64^3 grid points was used, resulting in a corresponding number of 67 108 864 particles. The time step is $\Delta t \, \omega_p = 0.01$ and the CPU time is close to $0.45 \, \mu$s per time step, per particle on the T3E computer using 64 processors. We have performed numerical simulations using periodic conditions in both x and y directions, and a circularly polarized plane electromagnetic wave is set in the whole box at time $t = 0$. Both plasma and fields satisfy the zeroth-order equilibrium given at the beginning of this paper. The initial distribution function was modified to include an oscillatory term in the p_y momentum:

$$f \left(x, y, p_x, p_y, t = 0 \right) = F_{\max} \left(p_x, p_y - eE_0 \cos \frac{k_0 x}{\omega_0^*} \right), \tag{29}$$

$$F_{\max} \left(p_x, p_y \right) = \frac{1}{2\pi v_{Tx} v_{Ty}} \exp\left(-\frac{p_x^2}{2m^2 v_{Tx}^2} \right) \exp\left(-\frac{p_y^2}{2m^2 v_{Ty}^2} \right). \tag{30}$$

We have perturbed all plasma modes (with an amplitude of 10^{-6}) to reduce the computational time. To make a comparison with results obtained in the 1D case, we again take the same parameter as used previously. Since the velocities are normalized to c and the frequency to ω_p, while the electromagnetic pump wave was chosen on mode $2 \, \Delta k_x$ (Δk_x being the fundamental mode in the x direction), the value of

$$k_0 = \sqrt{\frac{\omega_0^2}{\omega_p^2} - \frac{1}{\gamma_0}}$$

in fact determines the length of the system L_x in term of c/ω_p. The plasma length L_y ($= 2\pi/\Delta k_y$) is chosen in order to maximize the TPD growth rate and to reduce the computational time by taking $c \, \Delta k_y / \omega_0 \approx 1.20$. For these parameters, the growth rate of RMI reaches $\gamma_{RMI}/\omega_0 \approx 0.38$ for $(k_x c/\omega_0, \; k_y c/\omega_0) = (1.730, 0)$,

https://doi.org/10.1017/S0022377899008065 Published online by Cambridge University Press

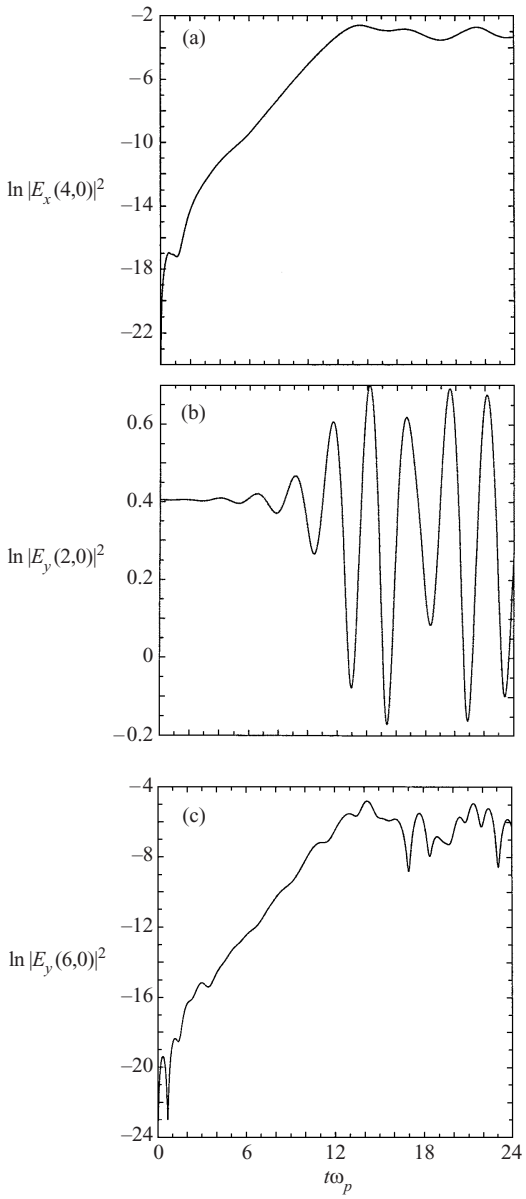

Figure 4. Time evolution of (a) mode 4 of the E_x electric field (plasma mode), (b) mode 2 of the E_y electric field (both pump and Stokes modes) and (c) mode 6 of the E_y field (anti-Stokes mode).

while $\gamma_{TPD}/\omega_0 \approx 0.28$ for $(k_x c/\omega_0,\ k_y c/\omega_0) = (2.60, 1.20)$, corresponding to TPD in a relativistic regime (see Fig. 6 of Quesnel et al. 1997b). Note that these values put the first mode Δk_y at $c\,\Delta k_y/\omega_p = 0.866$ in the region of maximum growth rate. Figure 4(a) shows the time evolution of mode 4 of the E_x field (plasma mode), Fig. 4(b) shows that of mode 2 of the E_y field (initially the pump wave), and Fig. 4(c) that of mode 6 of the E_y field. The E_z component is not shown here. A logarithmic scale is used here to represent the distribution function levels. The plasma

https://doi.org/10.1017/S0022377899008065 Published online by Cambridge University Press

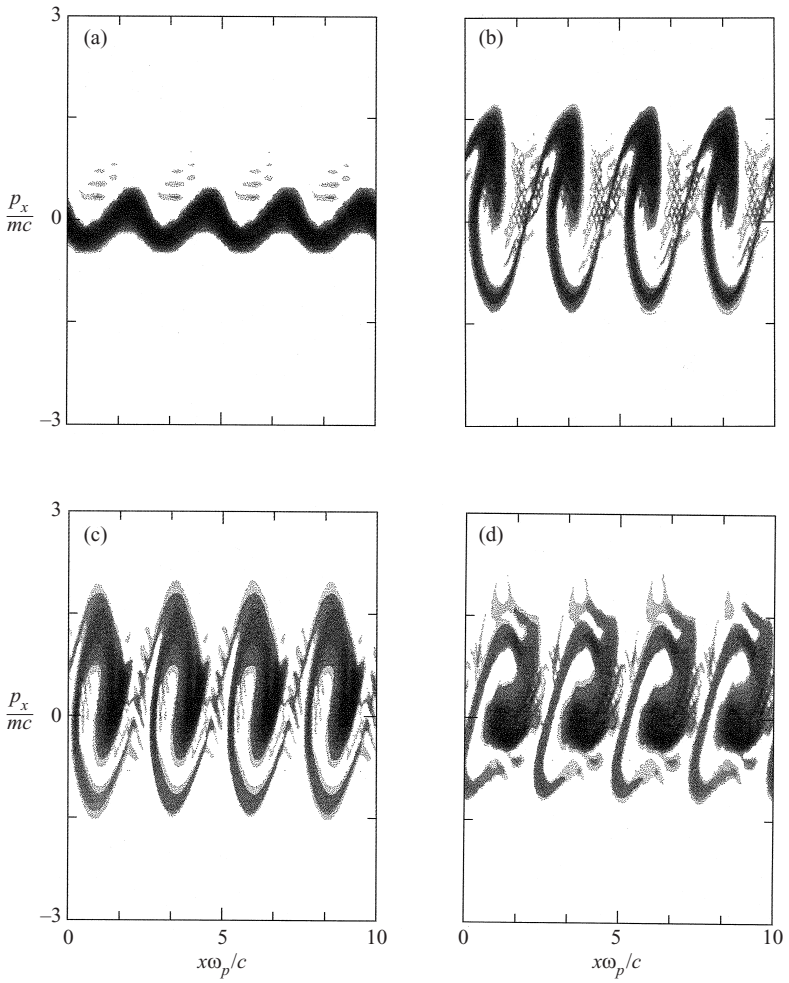

Figure 5. (x, p_x) phase-space plots of the distribution function at time $t\omega_p = 10$ (a), 14 (b), 16 (c) and 18 (d), showing clearly the strong modulation and particle trapping that is the signature of RMI. The numerical 2D Vlasov simulation was carried out with the same parameters as used in Fig. 1.

mode exhibits a numerical growth rate close to $\gamma_{\rm num}/\omega_0 \approx 0.38$, in very good agreement with the predicted value. Recalling that RMI is the result of the coupling of four waves, namely the pump wave (ω_0, k_0), the plasma wave (ω_e, k_e) and two electromagnetic scattered waves, the Stokes daughter (ω_s, k_s) and the anti-Stokes daughter (ω_{as}, k_{as}), the matching conditions are

$$\mathbf{k}_0 = \mathbf{k}_s + \mathbf{k}_e, \qquad \omega_0 = \omega_s + \omega_e, \tag{31}$$

$$\mathbf{k}_{as} = \mathbf{k}_0 + \mathbf{k}_e, \qquad \omega_{as} = \omega_0 + \omega_e. \tag{32}$$

Equations (31) and (32) determine the wavenumbers and frequencies of various modes once the pump wavelength has been given (we have taken here $ck_0/\omega_p \approx 1.225$). Analysing the solutions of the dispersion relation, we see that the growth rate is maximum for a value of the plasma wavenumber close to $ck_e/\omega_p = 2.353$ (with a real part of the frequency close to $\mathrm{Re}(\omega_e) \approx 0.46\omega_p$). From (31) and (32),

https://doi.org/10.1017/S0022377899008065 Published online by Cambridge University Press

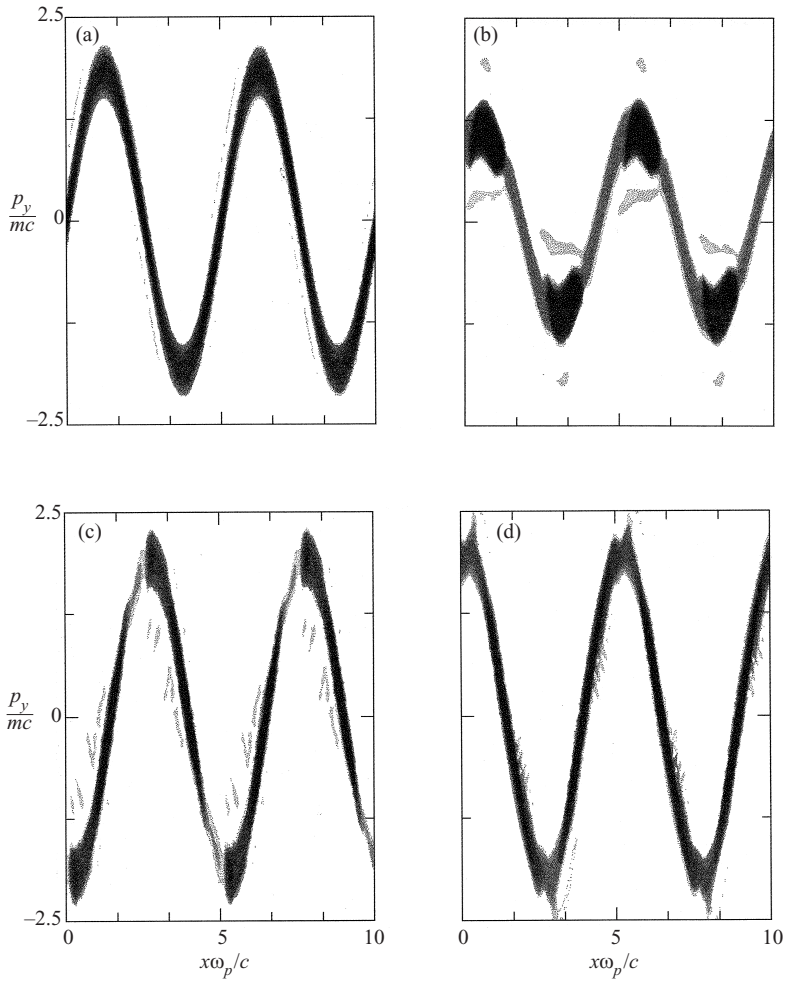

Figure 6. (x, p_y) phase-space plots of the distribution function (at the same times as in Fig. 5), illustrating the effect of the electromagnetic wave in the p_y direction. The modulation is due to the introduction of the $P_y\,(x, y)$ term in the initial distribution function.

the Stokes wavenumber is then $ck_s/\omega_p \approx -1.128$ ($\omega_s \approx 0.954\omega_p$) which is close to mode 2, while the anti-Stokes wavenumber is $ck_{as}/\omega_p \approx 3.758$ ($\omega_s \approx 1.874\omega_p$), corresponding approximately to mode 6. A perfect k-matching (since we have a periodic simulation) leads to a mismatch

$$\delta k_x = k_{as} - 6\,\Delta k_x = k_s + 2\,\Delta k_x = k_e - 4\,\Delta k_x \approx 0.097\frac{\omega_p}{c}$$

(with $c\,\Delta k_x/\omega_p = 0.6125$). Because both pump and Stokes modes are located on mode 2, Fig. 4 exhibits an oscillatory behaviour while the corresponding anti-Stokes mode (see Fig. 4c) has a strong growth with a growth rate estimated to be $\gamma_{\rm num}/\omega_0 \approx 0.375$. Note that the products of the instability are purely electrostatic for the plasma wave (with longitudinal polarization) and electromagnetic for the Stokes and anti-Stokes wave (with transverse polarization).

https://doi.org/10.1017/S0022377899008065 Published online by Cambridge University Press

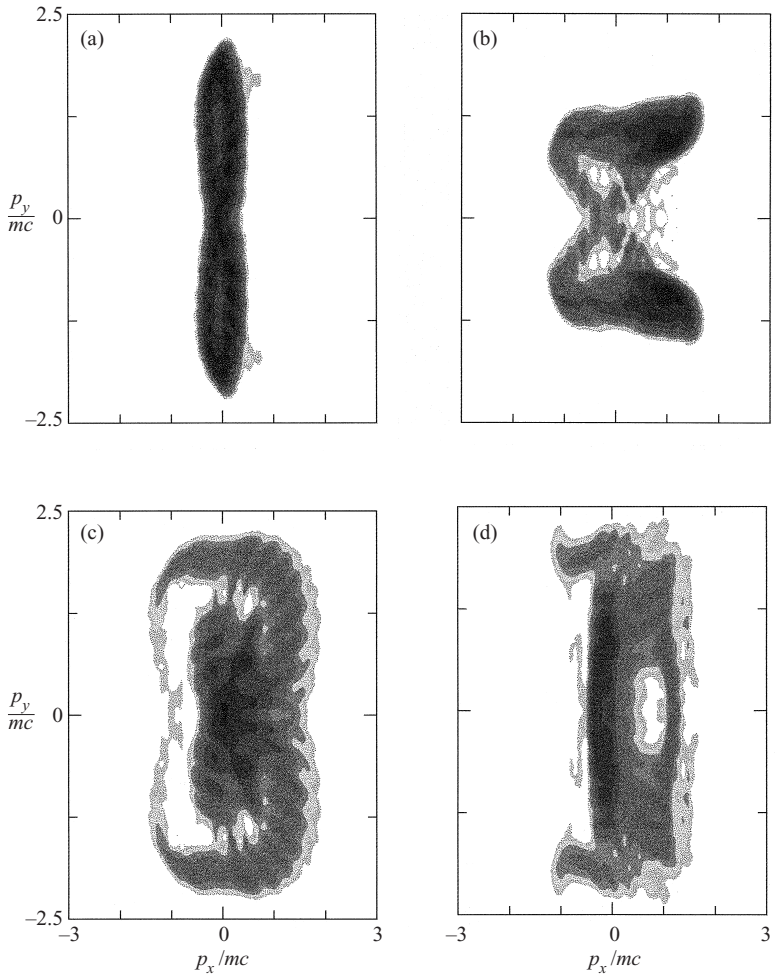

Figure 7. (p_x, p_y) momentum-space plots of the distribution function during plasma evolution (at the same times as in Fig. 5) showing the broadening of the distribution in the p_x direction.

4.2. Phase-space representation

A semi-Lagrangian Vlasov code allows precise comparison with the available theories: mode coupling, relativistic detuning and nonlinear saturation. The most striking advantage, however, of the Vlasov code (already demonstrated in a 1D open system – see Ghizzo et al. 1996a,b; Bertrand et al. 1995) is the very fine resolution in phase space, capable of resolving the finest mechanisms of particle dynamics. As our second example, we present phase-space results for the RMI case using 2D Vlasov simulations. In Fig. 5, phase-space contour plots are presented of the reduced distribution function $f\,(x, p_x)$ (integrated over y and p_y variables) at various times ($t\omega_p$ = 10, 14, 16 and 18). To improve the presentation of this diagnostic (and to accentuate the small values of the distribution function) a logarithmic scale has been used. The corresponding representations in (x, p_y) space and (p_x, p_y) space are illustrated respectively in Figs 6 and 7 at the same times. The curves at $t\omega_p$ = 10 correspond to the linear region of the instability, with a strong modulation of

https://doi.org/10.1017/S0022377899008065 Published online by Cambridge University Press

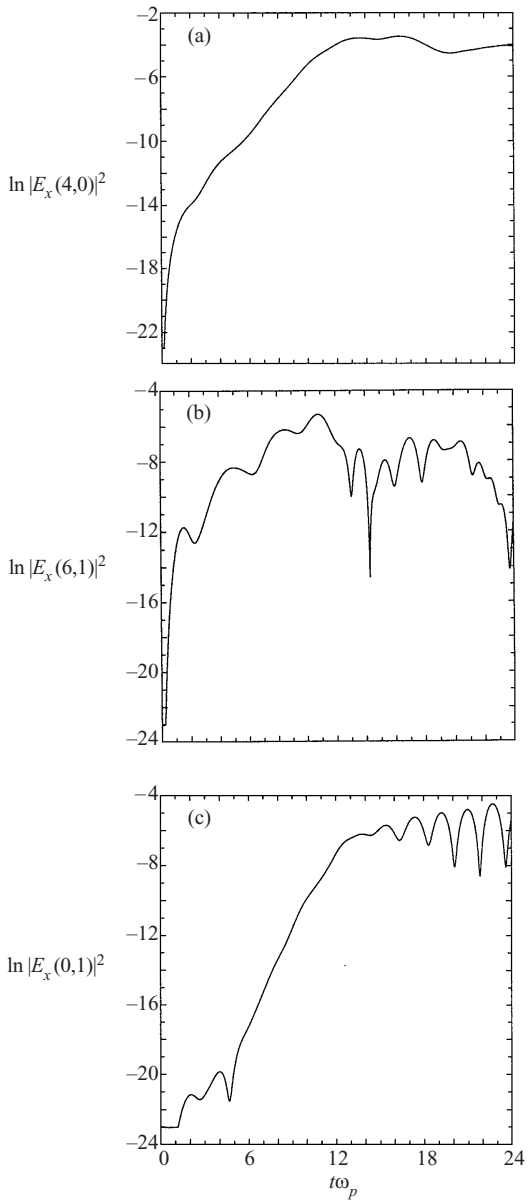

Figure 8. Time evolution of a selection of unstable modes on a logarithmic scale: (a) $E_x\,(4\,\Delta k_x, 0)$; (b), $E_x\,(6\,\Delta k_x, \Delta k_y)$; (c) $E_x\,(0, \Delta k_y)$. The corresponding growth rates, measured by the slopes of the curves, are respectively $\gamma/\omega_0 \approx 0.38$, 0.27 and 0.66. The last mode is due to mode coupling, and has a larger growth rate than that predicted by the linear theory.

the whole distribution function in (x, p_x) phase space. The modulation observed in (x, p_y) space corresponds to the electromagnetic modulation (via the term P_y) initially injected in the distribution function. The time $t\omega_p = 14$ corresponds to the beginning of the nonlinear phase of the development of RMI.

Owing to the very good resolution in phase space afforded by the Vlasov code,

https://doi.org/10.1017/S0022377899008065 Published online by Cambridge University Press

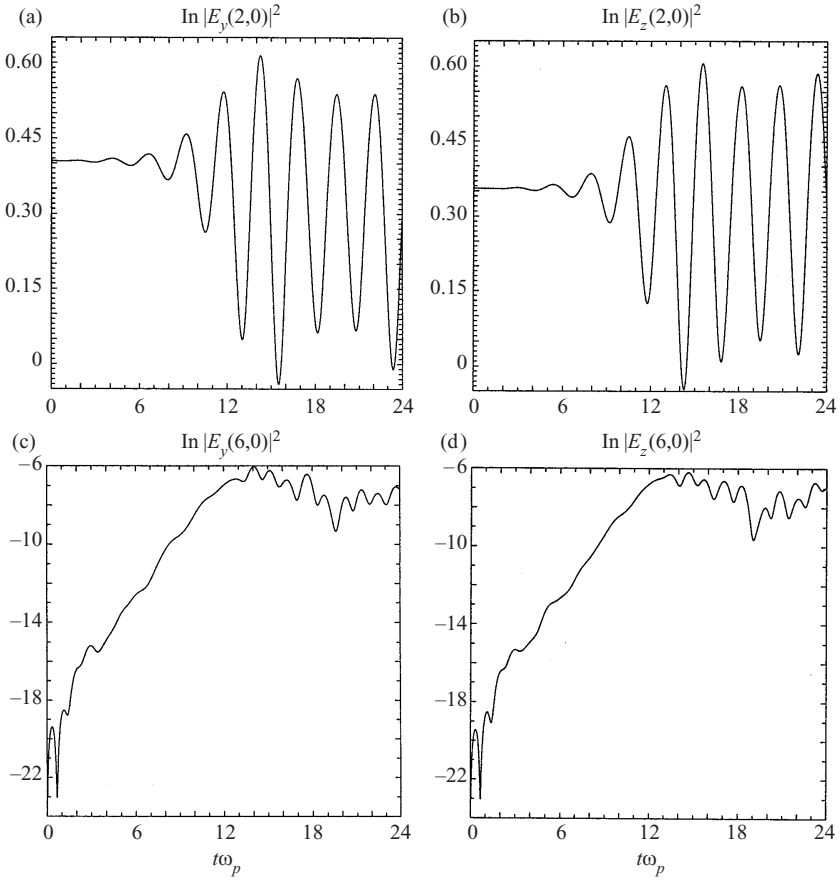

Figure 9. Time evolution of the y and z components of the electric field. (a) and (b) correspond to the mode $(2\,\Delta k_x, 0)$ (the circularly polarized pump wave mixed with the Stokes contribution). (c) and (d) are related to the mode $(6\,\Delta k_x, 0)$ (i.e. the anti-Stokes mode): the anti-Stokes mode increase gives rise to a numerical growth rate of $\gamma/\omega_0 \approx 0.36$, in good agreement with the theoretical value of $\gamma_{RMI}/\omega_0 \approx 0.38$.

one can begin to understand much of the details of the interaction. In keeping with the discussion of Fig. 4(a), one sees the appearance of (x, p_x) phase-space structures due to particle trapping in plasma wave. Note the formation of 'arms' corresponding to very a small level of the distribution function. Owing to plasma wavebreaking, there are regions in (x, p_y) space of high densities, as can be seen in Fig. 6 at time $t\omega_p = 14$. Now the description of the transverse behaviour of the distribution function by a Dirac distribution is not valid in that case. At time $t\omega_p = 18$, Fig. 6 shows clearly a break in the distribution function around $x\omega_p/c \approx 5$. We can note a small oscillatory behaviour in the p_y direction in time, with a perfect symmetry of f in this space. Owing to the strong modulation in (x, p_x) phase space, followed by particle trapping and the formation of vortices in this space, the distribution function broadens out in the p_x direction. Since the vortices remain coherent structures during plasma evolution without stochasticity generation, the instability does not lead to a heating process, which is an important result given by our Vlasov simulations.

https://doi.org/10.1017/S0022377899008065 Published online by Cambridge University Press

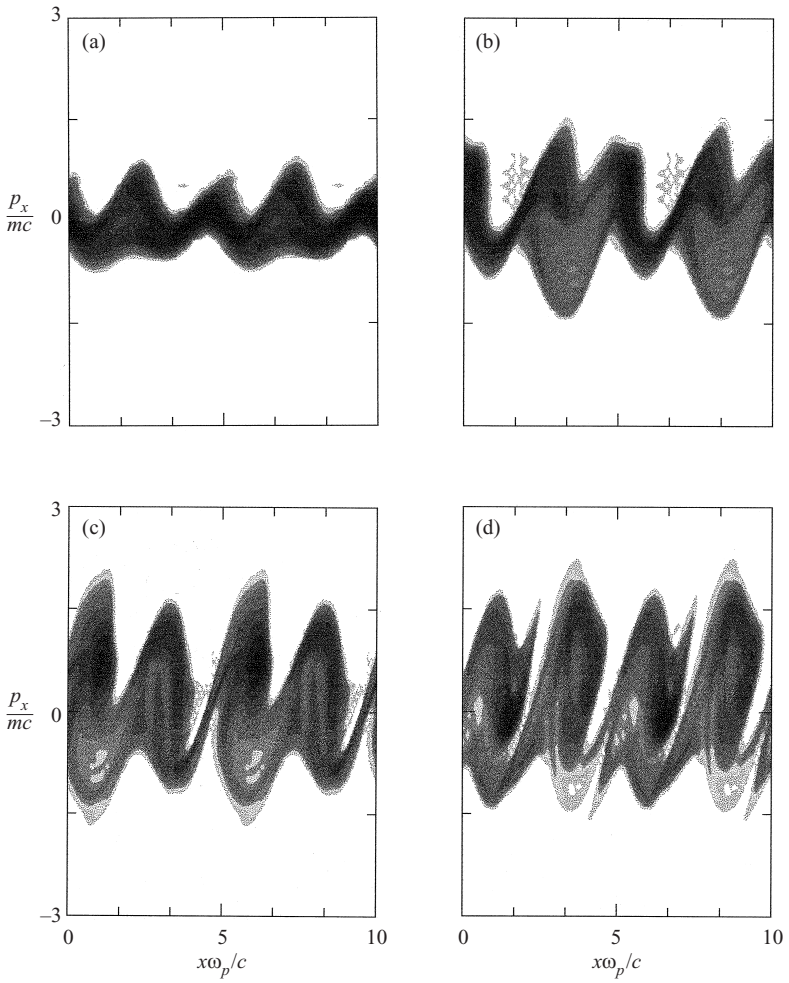

Figure 10 (a–d). For caption see facing page.

5. RMI and TPD coupling in the relativistic regime

5.1. Growth-rate estimation in the linear region of the instability

A second series of numerical simulations has been carried out in order to study the coupling between RMI and TPD in a relativistic regime. A detailed analysis of coupling, using the 2D dispersion relation, has been given by Quesnel et al. (1997b). They predict in the fully relativistic regime (in the case of parameters $n/\gamma_0 n_c = 0.25$ and $p_{\rm osc}/mc = \sqrt{3}$) a maximum growth rate of TPD ($\gamma_{TPD}/\omega_0 = 0.28$) for $(k_x c/\omega_0,\ k_\perp c/\omega_0) = (2.70, 1.20)$ (see Fig. 6 of Quesnel et al. 1997b). To confirm the preceding results, we keep exactly the values of the ratio of the electron density to the critical density and of the quiver momentum used by Quesnel et al. With these parameters, the first plasma wave appears with a wavevector $(k_{1x}c/\omega_p,\ k_{1y}c/\omega_p) = (3.818,\ 1.697)$ close to $(6\,\Delta k_x, \Delta k_y)$, with an error estimated as $\delta k_x = k_{1x} - 6\,\Delta k_x \approx -0.14\omega_p/c$. The second plasma wave (the daughter induced by TPD) is generated with a wave vector close to $(k_{2x}c/\omega_p,\ k_{2y}c/\omega_p) = (2.593, -1.697)$, which corresponds now to the Fourier mode $(4\,\Delta k_x, -\Delta k_y)$.

https://doi.org/10.1017/S0022377899008065 Published online by Cambridge University Press

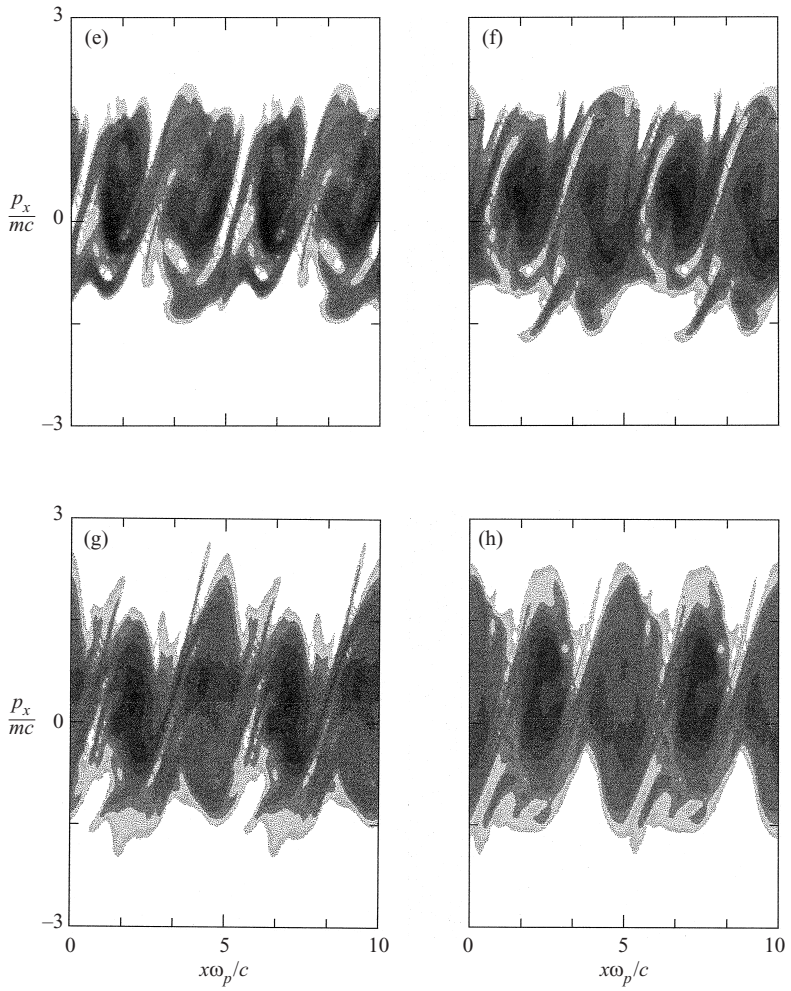

Figure 10. Coupling between RMI and TPD processes in the (x, p_x) phase-space representation afforded by the Vlasov code. While a four-wavelength structure can be observed without coupling (see Fig. 5), a more complex situation with loss of the phase-space structural coherence is now observed.

To start the TPD process, a perturbations in density are added on plasma modes $(6\,\Delta k_x, \Delta k_y)$ and $(4\,\Delta k_x, \Delta k_y)$ of 0.05 and 0.005 respectively (keeping a perturbation of 10^{-6} on the other modes to reduce the computational time). We observe the developments of the modes that are predicted to be unstable according to the previous results. Figure 8 shows the time evolution of a selection of unstable modes on a logarithmic scale: $E_x(4\,\Delta k_x, 0)$ in Fig. 8(a), $E_x(6\,\Delta k_x, \Delta k_y)$ in Fig. 8(b) and $E_x(0, \Delta k_y)$ in Fig. 8(c). The agreement is particularly good for the fastest-growing modes, which validates the theory. The coupling between RMI and TPD gives rise to a mixed polarization state of all modes involved in the parametric instabilities. All modes presented in Figs 8 and 9 are not restricted to be either longitudinal or transverse, but have a mixed polarization. The growth rates, determined by the slope of the curves presented in Fig. 8, have been estimated respectively as $\gamma_{\rm num}/\omega_0 = 0.38$ (in Fig. 8(a), the RMI branch), 0.27 (in Fig. 8(b), the TPD branch)

https://doi.org/10.1017/S0022377899008065 Published online by Cambridge University Press

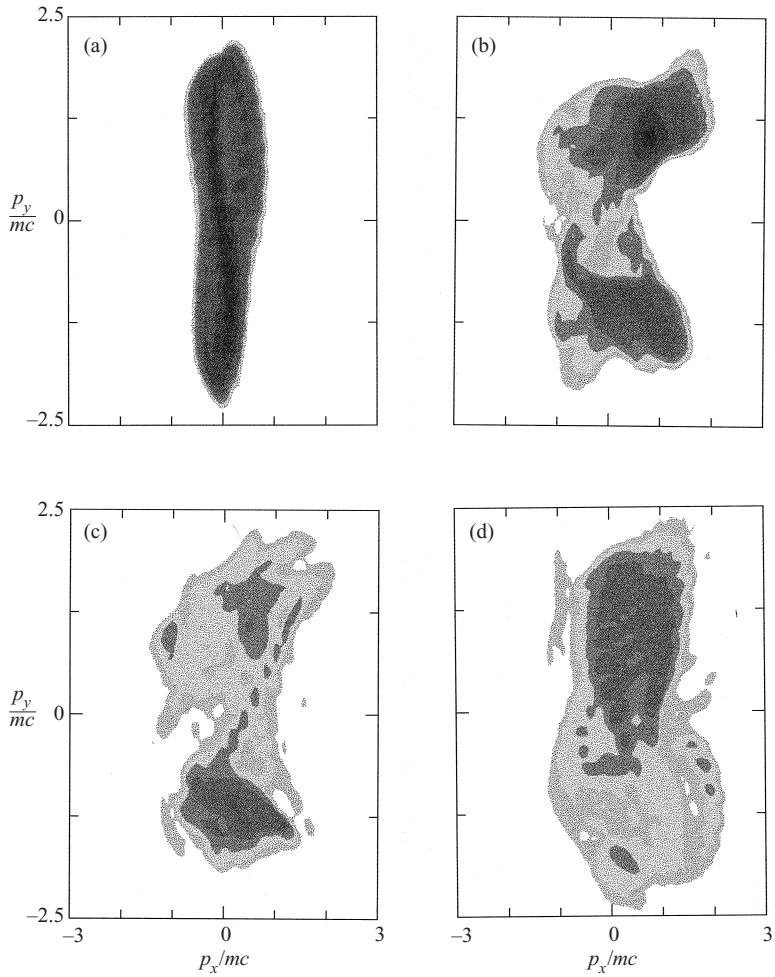

Figure 11. The (p_x, p_y) phase-space representation corresponding to Fig. 10 at times $t\omega_p$ = 10 (a), 14 (b), 22 (c) and 24 (d), showing the plasma evolution. Note that the momentum-space structure now becomes asymmetric.

and 0.65 (in Fig. 8(c), two times γ_{RMI}/ω_0). Note that we can observe in Fig. 8(c) the effect of mode coupling on the development of less-unstable modes. For instance, the mode $(0, \Delta k_y)$ has a growth rate larger than that predicted by linear theory, and is probably due to a coupling mechanism of type $(2\Delta k_x, 0) - (2\,\Delta k_x, -\Delta k_y)$. Figure 9 shows the time evolution of the E_y and E_z components of the electromagnetic field of mode $(2\,\Delta k_x, 0)$, corresponding to the pump wave (and also the Stokes mode), and of mode $(6\,\Delta k_x, 0)$, corresponding to the anti-Stokes mode. While Figs 9(a,b) exhibit the onset of the beat oscillatory behaviour with a strong modulation of the envelope of the pump wave, the anti-Stokes mode increases with a growth rate close to $\gamma_{\rm num}/\omega_0 = 0.37$ relevant to RMI.

5.2. Trapped particle dynamics in phase space

Further progress will depend on improving our understanding of wave–particle dynamics in the presence of several plasma waves that have been observed in the

https://doi.org/10.1017/S0022377899008065 Published online by Cambridge University Press

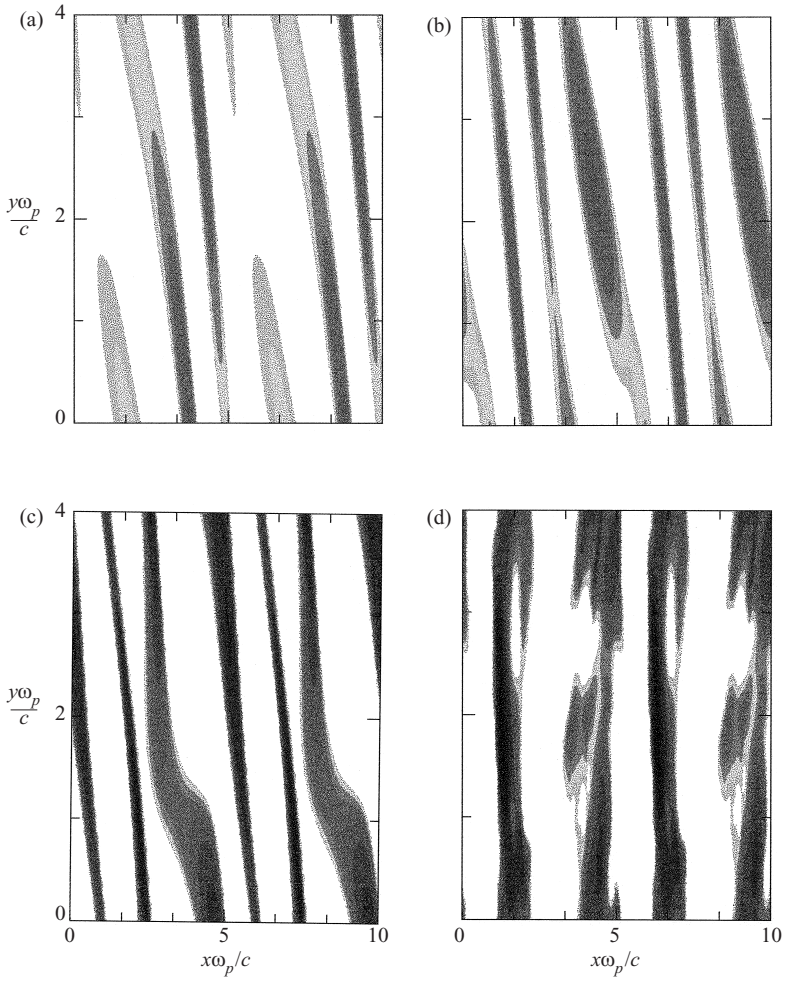

Figure 12. Further details of the plasma waves present in the plasma are illustrated here by showing the electron density at times $t\omega_p = 4$ (a), 6 (b), 10 (c) and 18 (d). The plots show clearly that the dominant plasma modes are $(4\,\Delta k_x, \Delta k_y)$ and $(2\,\Delta k_x, \Delta k_y)$.

Fourier-mode analysis. Here we give a detailed examination of such a coupling between RMI and TPD. The presence of the TPD process is due to the choice of the parameter $n/\gamma_0 n_c$ close to 0.25, while RMI is induced by relativistic effects. In Fig. 10 we have plotted the (x, p_x) phase-space representation afforded by the Vlasov code from time $t\omega_p$ =10 until 24 (using a time step of $2\omega_p^{-1}$). While a four-wavelength $(4\,\Delta k_x)$ structure for the plasma wave was found in the previous simulation, a more complex situation is now occurring owing to the presence of several plasma modes, which gives rise to the appearance of stochasticity in phase space. Further confirmation of this mechanism is provided by the plots of the distribution function in the (p_x, p_y) space (at times $t\omega_p$ = 14, 14, 22 and 24) shown in Fig. 11. We indeed see that the momentum-space structures become asymmetric while the TPD process goes on increasing in time. The strongly nonlinear regime of the instability (including RMI and TPD) differs radically from previous behaviour met in Sec. 4 due to the presence of the TPD process. More details of particle dynamics can

https://doi.org/10.1017/S0022377899008065 Published online by Cambridge University Press

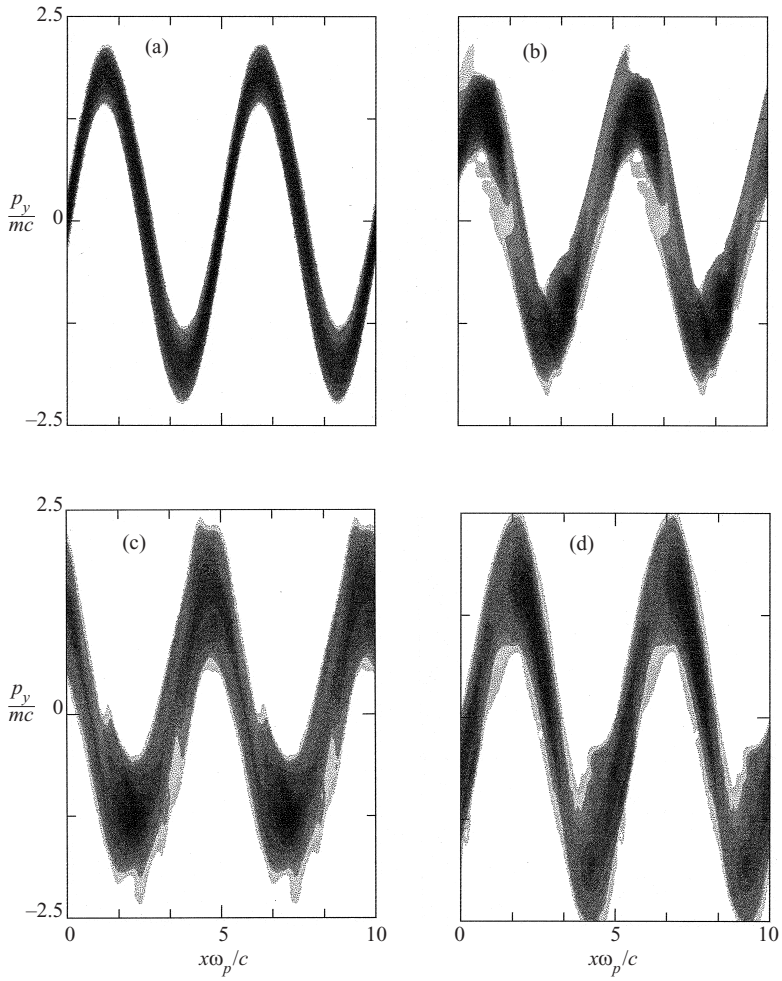

Figure 13. (x, p_y) phase-space representation afforded by 2D semi-Lagrangian Vlasov simulation in the case of RMI–TPD coupling.

be found in Figs 12 and 13, in which we have respectively represented the electron density and the distribution function in (x, p_y) phase space. Again the levels of the electron distribution function are represented on a logarithmic scale. Figure 12 illustrates the electron density behaviour at respective times $t\omega_p = 4$, 6, 10, 18, showing clearly that the dominant plasma modes are $4\,\Delta k_x$ and $2\,\Delta k_x$ in the longitudinal direction and Δk_y in the transverse direction. Figure 13 shows the evolution of a particle population in (x, p_y) phase space, which characterizes the transverse motion of electrons induced directly by the electromagnetic part of the laser field. Note that the phase-space structures remains coherent in this space.

In an earlier paper (Johnston et al. 1992) dealing with a 1D periodic plasma, we have shown that the Vlasov code is able to give strikingly clear pictures of phase-space dynamics, showing impressive correlation with simple orbit theory for steady waves. It should be noted that this is possible only when the accelerating waves are well defined and distinct as in stimulated Raman scattering. The phase-space portraits in general, however, contain a separatrix, so that orbits sufficiently near the

https://doi.org/10.1017/S0022377899008065 Published online by Cambridge University Press

separatrix are unstable to structural changes in the system. It is in this sense that a simple geometry is not trivial and contains the seed for chaos. If more than one plasma wave is involved (as here), with overlapping separatrices, one would expect Hamiltonian stochasticity from the resonance overlap. Even if the different plasma modes involved in the interaction process could be clearly identified, one would not know to which wave one should ascribe a given region of phase-space distribution, nor what frequency to use for computing the separatrix limiting trapped orbit trajectories. In effect, one could say that in the chaotic situation the waves could only quarrel over the electrons without being able to establish a clear title of ownership. The failure of coherence in Fig. 10 and of symmetry in Fig. 11 is not surprising, and indicates that the plasma behaviour cannot be inferred from only one plasma wave.

6. Conclusions

Detailed phase-space simulation results have been obtained using a $2\frac{1}{2}$D parallel semi-Lagrangian Vlasov code for the spatially periodic, initial-value parametric instability problem of the relativistic modulational instability and two-plasmon decay coupling. Growth rates in the linear regime of the instability have been satisfactorily verified for RMI and TPD in a strongly relativistic regime.

Although we have restricted ourselves to a few examples concerning RMI and TPD, striking pictures of the phase-space dynamics of particles have been obtained in a 2D system. The numerical simulations clearly show the formation of coherent vortex structures in phase space induced by the RMI process. These results should be a good starting point for understanding the final state and distribution of trapped or accelerated particles after the appearance of plasma wavebreaking. In cases where several plasma waves are present in the system, generally induced by RMI and TPD coupling, the plasma-particle distribution develops a more complex behaviour in phase space, with the onset of Hamiltonian stochasticity. It is clear that to describe the distribution function of trapped particles will require very detailed analysis of the kinetics and time history of plasma-wave evolution. Finally, obtaining this insight into the detailed behaviour was only possible with a semi-Lagrangian $2\frac{1}{2}$D Vlasov model, which can provide a great deal of resolution in phase space.

Acknowledgements

The authors are indebted to the IDRIS Computational Center, Orsay for time allocation on the Cray T3E and the Cray C98 computers. The authors are grateful to T.W. Johnston and M. Shoucri for very helpful discussions.

References

Afeyan, B. B. and Williams, E. A. 1997a Variational approach to parametric instabilities in inhomogeneous plasmas. III: Two plasmon decay. *Phys. Plasmas* **4**, 3827–3844.

Afeyan, B. B. and Williams, E. A. 1997b A variational approach to parametric instabilities in homogeneous plasmas. IV: The mixed polarization high-frequency instability. *Phys. Plasmas*, **4**, 3845–3862.

Adam, J. C., Héron, A., Guérin, S., Laval, G., Mora, P. and Quesnel, B. 1997 Anomalous absorption of very high intensity laser pulses propagating through moderately dense plasma. *Phys. Rev. Lett.* **78**, 4765–4768.

Bégué, M. L., Ghizzo, A. and Bertrand, P. 1998 Two dimensional Vlasov simulation of Raman scattering and plasma beatwave acceleration on parallel computer. Submitted to *J. Comput. Phys*.

Bertrand, P., Ghizzo, A., Johnston, T. W., Shoucri, M., Fijalkow, E. and Feix, M. R. 1990 A non periodic Euler–Vlasov code for the numerical simulation of laser–plasma beat-wave acceleration and Raman scattering. *Phys. Fluids* **B2**, 1028–1037.

Bertrand, P., Ghizzo, A., Karttunen, S. J., Pättikangas, T. J. H., Salomaa, R. R. E. and Shoucri, M. 1995 Two-stage electron acceleration stimulated Raman backward and forward scattering. *Phys. Plasmas* **2**, 3115–3129.

Birdsall, C. K. and Langdon, A. B. 1995 *Plasma Physics via Computer Simulation*. Institute of Physics Publishing, Bristol.

Coulaud, O., Sonnendrücker, E., Dillon, E., Bertrand, P. and Ghizzo, A. 1999 Parallelization of semi-Lagrangian Vlasov codes, *J. Plasma Phys*. **61**, 435–448.

Ghizzo, A., Réveillé, T., Bertrand, P., Johnston, T. W., Lebas, J. and Shoucri, M. 1995 An Eulerian Vlasov–Hilbert code for the numerical simulation of the interaction of high frequency electromagnetic waves with plasmas. *J. Comput. Phys*. **118**, 356–365.

Ghizzo, A., Bertrand, P., Lebas, J., Johnston, T. W. and Shoucri, M. 1996a A hybrid Eulerian Vlasov code, I, Study of high-frequency beatwave experiment and Manley–Rowe evolution in a finite causal system. *Phys. Plasmas* **3**, 650–667.

Ghizzo, A., Bertrand, P., Bégué, M. L., Johnston, T. W. and Shoucri, M. 1996b A Hilbert–Vlasov code for the study of high-frequency plasma beatwave accelerator. *IEEE Trans. Plasma Sci*. **24**, 370–378.

Guérin, S., Laval, G., Mora, P., Adam, J. C., Héron, A. and Bendib, A. 1995 Modulational and Raman instabilities in the relativistic regime. *Phys. Plasmas* **2**, 2807–2814.

Johnston, T. W., Bertrand, P., Ghizzo, A., Shoucri, M., Fijalkow, E. and Feix, M. R. 1992 Stimulated Raman scattering: action evolution and particle trapping via Euler–Vlasov fluid simulation. *Phys. Fluids* **B4**, 2523–2537.

Quesnel, B., Mora, P., Adam, J. C., Guérin, S., Héron, A. and Laval, G. 1997a Electron parametric instabilities of ultraintense short laser pulses propagating in plasmas. *Phys. Rev. Lett*. **78**, 2132–2135.

Quesnel, B., Mora, P., Adam, J. C., Héron, A. and Laval, G. 1997b Electron parametric instabilities of ultraintense laser pulses propagating in plasmas of arbitrary density. *Phys. Plasmas* **4**, 3358–3368.

Sakharov, A. S. and Kirsanov, V. I. 1997 Stimulated scattering of relativistically strong radiation from an underdense plasma at high-frequency harmonics. *Phys. Plasmas* **4**, 3382–3389.